QUANTIFYING TERMINAL WHITE BANDS IN SALIX FROM THE YENISEI RIVER, SIBERIA AND THEIR RELATIONSHIP TO LATE-SEASON FLOODING

Richard D. Thaxton*[a,b], Irina P. Panyushkina [a], David M. Meko [a], Georg von Arx[c,d], Leonid I. Agafonov[e]

[a]Laboratory of Tree-Ring Research, University of Arizona, Tucson, AZ, USA, [b]School of Natural Resources and the Environment, University of Arizona, Tucson, AZ, USA, [c]Swiss Federal Institute for Forest, Snow and Landscape Research WSL, Birmensdorf, Switzerland, [d]Oeschger Centre for Climate Change Research, University of Bern, Bern, Switzerland, [e]Institute of Plant and Animal Ecology UB RAS, 202 Marta 8th St., Yekaterinburg, 620144, Russia

*Corresponding author: rthaxton@email.arizona.edu

Highlights

- *Salix alba* trees growing along the lower reaches of the Yenisei River display terminal white bands, a type of intra-annual density fluctuation (IADF) where whiter wood appears at the end of certain growth rings

- Previous work has shown terminal white bands in ring-porous species reflect late-season flooding, but it is unknown if this is also true for diffuse-porous species

- Quantitative wood anatomy (QWA) was used to quantify these terminal white bands via measurements of lumen area (LA) and cell wall thickness (CWT) of wood fibers

- QWA data and consecutive days of high-water levels in July are correlated in some trees

- Terminal white bands in this system may be caused by July floods, which have diminished in the system since 1980

Abstract

Recent, record-breaking discharge in the Yenisei River, Siberia, is part of a larger trend of increasing river flow in the Arctic driven by Arctic Amplification (AA). These changes in magnitude and timing of discharge can lead to increased risk of extreme flood events, with implications for infrastructure, ecosystems, and climate. To better understand the changes taking place, it is useful to have records that help place recent hydrological changes in context. In addition to an existing network of river gauges, wood anatomical features in riparian trees have been shown to record extreme flooding. Along the lower reaches of the Yenisei River we collected white willow (*Salix alba*) samples from a fluvial fill flat terrace that occasionally floods when water levels are extremely high. At the end of certain annual growth rings these samples displayed terminal white bands, a type of intra-annual density fluctuation (IADF). To identify the characteristics and causes of these features we use an approach known as quantitative wood

anatomy (QWA) to measure variation in fiber cell dimensions across tree rings, particularly fiber lumen area (LA) and cell wall thickness (CWT). We investigate (1) which cell parameters and method to extract intra-annual data from annual tree rings best capture terminal white bands identified in *Salix*, and (2) if these patterns are related to flood magnitude and/or duration. We find that fiber CWT best captures the IADFs found in *Salix* rings. For some trees, time series of normalized CWT correlate with July flood durations, which have changed since the 1980s. Understanding how riparian vegetation responds to extreme flood events can help us better manage riparian ecosystems and understand changes to the Arctic hydrological regime.

Keywords: quantitative wood anatomy; wood fibers; intra-annual density fluctuation; Yenisei River Basin; hydrology

Introduction

River discharge in the pan-arctic has intensified over the last century and will likely continue to change in coming decades (IPCC, 2021). Hydrological changes are driven by Arctic Amplification (AA) - a positive feedback loop of accelerating warming over the Arctic resulting in a combination of increasing surface air temperature, melting of sea ice and permafrost, and increased precipitation in northern latitudes (Screen and Simmonds, 2010; Shiklomanov et al., 2013). This forcing is able to produce record-setting river discharge that is part of an accelerating trend (Shiklomanov and Lammers, 2009). Although hydrological changes across and within river basins are heterogenous, the net effect is an increase of freshwater export to the Arctic Ocean in spring, summer and even winter (Feng et al., 2021; Panyushkina et al., 2021). There are strong expectations for these trends to continue during the rest of the 21st century (Carmack et al., 2016; Bring et al., 2017; Zanowski et al., 2021). On the global scale, these changes may have critical implications for ocean circulation (Serreze and Francis, 2006; Jones et al., 2008; Weijer et al., 2020, but see He and Clark, 2022), global climate (Coumou et al., 2018), and human trade and navigation (Smith and Stephenson, 2013). On the ecosystem and plant scale, increased flooding will potentially alter Arctic ecosystem function and impact plant physiology (Fan et al., 2020).

Tree rings can be instrumental for providing long-term context to more frequent floods and altered hydrology (Meko et al., 2012; Ballesteros-Cánovas et al., 2015). Existing instrumental discharge records in the Arctic are often sparsely located and for limited duration, creating a need for additional data (Bring et al., 2017). Tree ring records derived from conifers have been used to successfully extend discharge records across the pan-Arctic by hundreds of years (MacDonald et al., 2007; Agafonov et al., 2016). These studies not only provide critical insight into long-term annual discharge trends, but seasonal trends as well (Panyushkina et al., 2021). Dendrochronology of angiosperms offers an opportunity to fill even more of these gaps, particularly when it comes to capturing extreme hydrological events. Angiosperm wood anatomical response to flooding is dependent on both the timing and magnitude of the discharge. The

largest floods tend to have a direct effect on vegetation via impact and scarring, with floods recorded as reduced xylem vessel lumen area or increased fiber lumen area in the injured ring (Ballesteros et al., 2010; Arbellay et al., 2012). Even if the tree is not physically injured, flood events can still be recorded in tree rings. Most research into angiosperm anatomical response to non-injurious flooding relies on vessel measurements from ring porous species (trees with distinct earlywood and latewood) (Ballesteros-Cánovas et al., 2015). Anomalous rings formed during peak spring discharge tends to produce earlywood vessels of reduced size which can be identified visually and can help understand flood history (Meko and Therrell, 2020; Nolin et al., 2021). Even small changes in vessel size are physiologically important since small increases in diameter can greatly increase hydraulic conductivity, as illustrated by the Hagen-Poiseuille law (Tyree and Ewers, 1991). Chronologies of vessel area and vessel number are particularly useful for capturing large spring discharge because, unlike ring width, the relationship is maintained even for very large discharges (Kames et al., 2016). The caveat is that only a short window (2-3 weeks) exists for the tree to record this information, limiting its utility (Kames et al., 2016).

When researchers have used diffuse porous angiosperms (no clear separation of earlywood and latewood) to study flood history, they typically rely on vessel characteristics. Diffuse porous species response to flooding is varied, appearing to vary by species and biome. For example, recent work with *Alnus glutinosa* showed no relationship between prolonged flood events and vessel characteristics (Anadon-Rosell et al., 2022). In contrast, Lopez et al. (2014) examined the tropical species *Prioria copaifera* and found chronologies of vessel number could be used to reconstruct flood height, as most radial growth occurred during flood years (López et al., 2014). Other studies have even related vessel distribution (i.e. tangential vessel bands) to prolonged flood inundation (Tardif et al., 2021).

While the utility of vessel elements appears well established there is a need to understand the utility of other wood cellular components such as wood fibers. Fibers form the structural component of the wood, and, although little or not involved in the actual xylem transport of water, are still important to water movement up the stem. Exploration of fibers is still in its infancy, but interest in growing. Research into the flood response of riparian *Salix* trees along the Ob River, Siberia revealed extreme flood events were captured as extremely narrow rings or rings with sudden changes in wood fibers (Meko et al., 2020). Wood fibers have also been reported to be as sensitive to environmental fluctuations as vessel chronologies, confirming their utility (De Micco et al., 2016). However, they may not be useful for every research question, as wood fiber measurements of flooded alder showed no relationship between extreme flooding and cell wall thickness (CWT) (Anadon-Rosell et al., 2022). Still, some research does suggest wood fibers have the capacity to record flood events, at least for ring porous species. The most relevant study is work by Yanosky (1984) which related increased wood fiber size and decreased cell wall thickness near the end of the annual growth ring to flooding events late in the growing season. This study, which examined riparian ash (*Fraxinus*) near Washington, D.C., USA, found

3

white bands appeared more frequently in flood years, and hypothesized that these fluctuations were essentially 'growth spurts' in which flooding of the root zone allowed drought-stressed trees to take advantage of additional water. Fluctuations tended to occur most often when the tree was younger and appeared on the wood surface as a white terminal band forming before the earlywood of the following year (Yanosky, 1984).

We identified rings similar to those described by Yanosky in wood samples of diffuse-porous *Salix alba* (white willow) sampled in the summer of 2020 along the Yenisei River, Siberia. These rings only showed changes in wood fibers and were unaccompanied by any equivalent abnormal vessel patterns. Given these anomalies' potential relationship to late-season flooding, they may prove useful for understanding flood variability in this globally-important watershed. Additionally, since these white bands represent changes in fiber characteristics, investigation into these wood anomalies offers a chance to provide much-needed research into quantifying physical characteristics of wood fibers in diffuse porous species. Recent advances in the field of quantitative wood anatomy (QWA) offer an opportunity to measure characteristics of these white terminal bands at the level of individual cells, building time series to compare with hydrologic data. Understanding intra-annual variation in tree rings allows us to probe into subtle, intra-annual changes in the basin's hydrology. For these reasons, we investigated the characteristics of terminal white bands identified in Salix rings and explored (1) which QWA measurements (cell wall thickness (CWT) or lumen area (LA)) and which intra-annual data extraction methods allow us to best quantify these anomalies, and (2) how white bands relate to flood magnitude and duration. We hypothesized that fiber cell wall thickness would better capture these features than fiber lumen area, which would be further improved when cell wall thickness of each cell is normalized by the average cell wall thickness of the ring. Additionally, we expected that averaging cells based on their absolute position in the ring would better quantify white bands than using the relative position. With the best combination of cell measurements and methods we hypothesized there would be a relationship between terminal white bands and flood events late in the growing season. Understanding how best to measure these unique features can help us better attribute their cause, and may improve our understanding of short-lived intra-annual hydrologic events throughout the lower Yenisei River basin and their effect on vegetation.

Materials and methods

1. Characterization of study site, climate and river discharge

The study site (Figure 1) is located on an island (   ) at the confluence of the Turukhan and Yenisei Rivers, roughly 10 km downstream from the city of Turukhansk (Siberia, Krasnoyarsk Krai; 65.856 N, 87.736 E). A riparian forest dominated by *Salix alba* (white willow) exists at the top of this terraced island, roughly 12-15 meters above the median water level, excluding the June-July flood period (3.6 m asl). In general, the forest forms an open canopy with a dense understory of herbaceous plants and grasses. The elevation of the top of

4

the island does not vary more than a meter over the study site.

The climate of this area is classified as continental sub-artic, with mild summers and extremely cold winters (Beck et al., 2018). The closest climate station with monthly data is Turukhansk, 12 km southeast of the study site (WMO Code 23472, *GHCN-M v3.3.0.20190817*, 65.78 N, 87.93 E, elevation: 64 m). Mean monthly temperatures (1891-2019) range from -26 to 15 ˚C, peaking in July, and the site receives almost 550 mm of precipitation annually (1881-2018). The growing season for these trees typically lasts from mid-May to early September. Climatological and hydrological information is summarized in Supplemental Figure 1.

Discharge in the Yenisei River is driven by snowmelt with peak flows typically occurring in early June (Supplemental Figure 1c). Water level data was obtained from a site at Selivanikha 6 km east and just downstream of the study site (gauge code 9801; 65.862126 N, 87.865896 E). Although water levels can reach 22 m during peak flows, the median annual maximum water level is 17.5 m (Supplemental Figure 2). Additionally, water levels above 14 m do not typically last longer than a month. While July flows pale in comparison to the massive discharge in June, important changes in water level and flood duration are still evident (Figure 2). July flows have decreased to the point July water levels have not reached 10 m since 1992, despite this being a frequent occurrence prior. Extensive dam construction during the 1980s in the upstream portions of the basin is the likely culprit behind these late summer changes.

2. Tree sampling, wood processing and ring width chronology development

In August 2020, we collected cross-sections from 7 willow trees using a chainsaw, targeting dominant trees that appeared noticeably older. These trees were the largest and dominant woody vegetation on the top of the island, comprising a forest with wide spaces between trees and with an extensive understory of herbaceous plants. Trees were sampled in close proximity to each other, no more than 10-20 m apart. Wood discs were cut between 0.7 and 0.8 meters above the ground. The wooden disks were transported to the Laboratory of Tree Ring Research in Tucson, Arizona for subsequent preparation. All slabs were sanded using a belt sander with progressively finer grits of sandpaper (80-400 grit). We dated and measured two radii, separated by 90-180 , on each slab. Each ring was assigned a calendar year, and cross-dating of samples was performed both visually and with skeleton plots (Stokes and Smiley, 1968). Ring widths were measured using a Lintab translational stage and TSAP-WIN software (Rinntech; Heidelberg, Germany). The program COFECHA was used for quality control of the measured ring widths (Holmes, 1983).

The resulting chronology was built by averaging the detrended ring widths of each series using the R package dplR (Bunn, 2008). Each ring width series was detrended using a modified negative exponential curve if supported by the data, otherwise a straight line with positive or negative slope was fit. This detrending method was preferred because the majority of series did not exhibit

the typical growth trend of declining tree ring width with age. Instead, most series showed low growth over the first 20-40 years, followed by an increase in growth that was sustained over most of the remaining length of the series. Spline detrending tended to remove this pattern, which was likely not related to the effect of tree growth over an increasing stem circumference. This lack of an obvious age trend coupled with the short length of most series made the negative exponential preferable over other detrending methods. We used the program SEASCORR (Meko et al., 2011) to investigate the relationship between tree growth and climatic factors from 1950-1993, including discharge (Yenisey at Igarka, station code 9803, 67.43 N, 86.48 E), mean monthly temperature and total monthly precipitation. We used the 'ggplot2' package for graphical display (Wickham, 2009).

3. Characterization of White Bands

In addition to the ring width chronology, we qualitatively and quantitatively characterized each terminal white band as they appeared on thin sections (see below). First, we developed a character list identifying years where white bands at any position in the growth rings occurred (Yamaguchi, 2011). We classified anatomical anomalies on if they occurred in the 'early' or 'late' portion of the growth ring, a classification scheme similar to how angiosperm IADFs are characterized in other research (De Micco et al., 2016). The total number of trees showing terminal white bands were then tallied for each year to build a frequency histogram. It is worth noting that 2001 was an anomalous 'white ring' that appeared in every tree. Unlike the white bands described by Yanosky, the entirety of the 2001 ring appeared white. Past research has linked these features to extreme, early-season defoliation events, possibly as a result of an insect outbreak (Hogg et al., 2002; Prendin et al., 2020). This feature, though interesting, displayed no obvious intra-annual variation and so was excluded when categorizing rings with white bands.

We also measured the width of each visually-identified white band. Measurements were made on an image of the tree in Image-Pro Plus (v6.1; Media Cybernetics) on the same portion of the tree chosen for thin sectioning. Each band was measured at four different locations along the ring and averaged together to create one width value per ring. We then used Pearson correlations to investigate if a relationship existed between terminal white band width and ring width. The relationship between ring width and terminal white band width affects how to best quantify attributes of these bands. If white band width is a function of ring width, we need to account for the width of the ring in our measurements of white bands. This can be accomplished by calculating the relative position of white bands (dividing the bands position by the total ring width). Alternatively, if terminal white bands are independent of ring size, white bands are best characterized by a fixed width and knowing its absolute position in the ring is adequate.

3. Anatomical sample preparation and quantitative wood anatomical analysis

All samples were prepared for quantitative wood anatomy using similar procedures to those found in other research (Edwards et al., 2020; Anadon-Rosell et al., 2022). Each slab was cut radially into ~1 cm wide radial bars that included the center of the slab. Each core was then cut tangentially into 5-9 pieces, depending on the diameter of the tree. A 12 µm thin section was then cut from each piece using a rotary microtome (Thermo Scientific Microm HM 355S Microtome, Waltham, MA). To ensure adequate contrast between anatomical features and background of images, thin sections were stained with cresyl violet acetate (0.5 grams per 250 ml H_2O). After letting the stain sit for 30 minutes, fresh stain was applied to all samples and let sit for an additional 10 minutes. Each slide was then rinsed with solutions of increasing ethanol concentration (50%, 100%) and permanently affixed to the slide using Eukitt mounting medium. Slide imaging was performed at the Swiss Federal Institute for Forest, Snow and Landscape Research WSL (Birmensdorf, Zürich, Switzerland) using a Zeiss Axio Scan Z1 (Carl Zeiss AG, Germany).

From each tree, thin section images from at least 1965-1980 were selected for further analysis because the majority of visually identified terminal white bands occurred in this time frame. Automatic detection of wood fibers from images was performed using ROXAS (von Arx and Carrer, 2014). While the program's utility has been demonstrated countless times for conifers, it is also very effective for identification of anatomical features in diffuse porous species, such as vessels (von Arx et al., 2013; Wegner et al., 2013; Anadon-Rosell et al., 2022). ROXAS allows users to filter out cells of particular sizes, allowing us to investigate fiber characteristics separate from vessels. Vessels in our samples were determined to generally have a lumen area between 500-12000 µm² (von Arx, Personal communication) so all cells with an area $>=500$ µm² were removed when investigating fibers. For each image we then performed manual correction of the ROXAS-identified cells. Any improperly identified cells (e.g. fiber cell identified as vessel or ray parenchyma), or cells with collapsed cell walls were deleted. All ring borders were drawn manually because ROXAS' automatic ring boundary detection is unreliable when cell size and density transitions are subtle (Wegner et al., 2013). ROXAS-derived ring width measurements were compared to manually-measured ring widths to ensure each ring was assigned to the proper calendar year. Upon completion of manual user correction, output excel documents for each image and cell type were created with multiple measured parameters. For subsequent analysis, only fiber LA and CWT were considered.

4. Data processing and statistical analysis

We developed an R script modified from the SECTOR.R code developed by Richard Peters (https://deep-tools.netlify.app/2020/11/24/sector-intro/). This approach is similar to that employed in the R package RAPTOR used to read, prepare and visualize anatomical data from conifer tracheids (Peters et al., 2018). The code allowed us to read all ROXAS output for each tree, remove anomalous data, and re-calculate cell positions if imaged ring boundaries were not

completely horizontal.

To determine how to best quantify the terminal white bands in our samples, we compared multiple approaches. The first approach was based on the direct measurements of terminal white band widths. For all white bands we determined the mean white band width (157.7 µm, = 8.9 µm, n = 131) and the minimum width (50 µm) for all trees. Using modified SECTOR code, we created time series of cell measurements averaging cells between the minimum or average white band width and the ring boundary. The benefit of this approach was that it was derived from the characteristics of the white bands, allowing us to specifically target these anomalies.

We also employed a sectoring approach similar to that used in other studies (Edwards et al., 2020; Gebregeorgis et al., 2021). This approach divides the ring into n equal radial sectors, where each sector is $100/n\%$ of the total ring width. Cells were assigned to a particular sector if their relative radial position fell within the range of values for that sector. The cell parameter (i.e. LA or CWT) value of all cells within a particular sector were then averaged together to produce one cell parameter value per sector. To determine which sector best captured the terminal white bands, rings were sectored into $n = 8$, 10, or 20 equal-sized pieces and the value from the nth sector was compared between rings where we did and did not visually identify a terminal white band. These values for n were chosen because each would sector an average ring (1.8 mm or 1800 µm wide, years 1950-2020) into widths within the range of those identified for terminal white bands. For example, dividing a ring into 10 sectors would mean each sector would have a width of $1800/10 = 180$ µm. The sectoring approach might be helpful to match relative intra-ring position with seasonal wood growth phenology because ring width is variable from year to year and cells in different rings that are the same distance from the ring boundary may have formed at different times. For each method above, we also normalized cell parameters to further improve quantification of white bands. Prior to averaging all cell measurements (CWT, LA) within a sector, measurements of each cell were divided by the average cell measurement for the entire ring. The normalized measurements were compared to non-normalized (absolute) measurements for each sectoring approach.

To assess which method best agreed with our visual identification of terminal white bands, we used biserial correlation to estimate the relationship between the presence of terminal white bands and measured cell parameters (Bedrick, 2005). The biserial correlation is an estimate of the product-moment correlation in the case where one variable is dichotomous (e.g. presence/absence) and the other is continuous (e.g. CWT). Correlation coefficients derived using this method are commensurate to r values derived using Pearson correlations (Jacobs and Viechtbauer, 2016). The method assumes both sets of data have normal distributions, have few outliers, and the variances are approximately equal, although the test is robust to data with different variances. We used various statistical tests in R to test for each of these assumptions. We tested

if each group of data had normal distributions using the Shapiro-Wilk's test in the stats R package (Shapiro and Wilk, 1965; Royston, 1995), and tested for equal variances between the two groups using Levene's test in the car R package (Brown and Forsythe, 1974; Gastwirth et al., 2009). We used boxplots to identify outliers and histograms to visually assess the distributions of each group. The biserial correlation was calculated using the biserial.corr function from the ltm R package (Rizopoulos, 2007). All analyses were performed using R Statistical Software (v3.6.3; R Core Team 2020)

After determining which cell measurement and sectoring method best captured the terminal white bands, we created time series using the best combination. To determine if cell parameter chronologies could be built from each tree, we compared series from different trees with Pearson correlations and tested if they were significant. Given the short length of these time series, more robust statistical tests were not possible. Additionally, we calculated the Pearson correlation coefficient between each tree's time series and climatic and hydrologic variables, including water level, duration of flooding at a particular water level, mean daily temperature & daily precipitation (Igarka, RSM00023274, 67.47 N, 86.57 E) (Menne et al., 2012), and water temperature.

Results

1. Relationships of tree ring growth with climate and river discharge

The interseries correlation of all seven tree ring series was 0.61 for years 1940-2020, confirming trees agreed in their patterns of annual growth. Although the resulting chronology extends from 1897-2020, it is not robust before 1940 as the sub sample signal strength falls below 0.9 before then (Bunn, 2008; Buras, 2017). 4 of the 7 trees had center rings dating between 1941-44, and the youngest tree had a center ring dating to 1952. From 1950 on, tree growth tended to gradually increase before seeing a steep decline from 2003-present (Figure 3).

Correlations calculated in SEASCORR show a significant negative relationship (r = -0.4, alpha=0.01) between tree growth and monthly discharge (primary variable) in July, and partial correlations show a significant positive relationship (r = 0.5, alpha=0.01) with mean temperature (secondary variable) in June, when the intercorrelation of temperature and discharge has been adjusted for (Supplementary Figure 3). This relationship between growth and July discharge appears to be linear and is significant at this site (r = 0.42, p < 0.05; Supplemental Figure 4). When discharge is replaced with precipitation as the primary variable, there is also a significant negative relationship (r = -0.4, alpha=0.01), but in the month of June.

2. Macroscopic characteristics of white bands in Salix

Rings with terminal white bands could be easily distinguished from years with normal growth (Figure 4). White bands in the 'late' portion of the ring were more consistent between trees than those in the 'early' portion, and so we decided to focus on those anomalies. A frequency histogram of early and late

9

IADFs, and examples of those IADFs, are shown in Figure 3c. Between 1950-2020, late IADFs were found in over half the years (57% of years) in minimum one tree and, on average, there were 1.4 white bands per year for all seven study trees combined. Occurrence of terminal white bands peaked in years 1951-53 and 1959-60. Following these years the frequency of terminal white bands declined toward the present and almost no white bands were identified after the mid-1980s. There were also important differences between the number of white bands identified per tree (Table 1). For example, tree BSH04 had 23 white bands between 1950-2020, but BSH07 only showed 1.

Information on terminal white bands per tree is summarized in Table 1. The measured widths of white bands were consistent between trees, and widths ranged from 50-600 µm. There was only weak evidence that white band width was related to ring width. Trees BSH01-3 showed varied and positive relationships between white band width and ring width ($r_1 = 0.32$, $p_1 = 0.33$; $r_2 = 0.52$, $p_2 = 0.01$; $r_3 = 0.41$, $p_3 = 0.05$), but trees BSH04-6 showed no relationship ($r_4 = 0.07$, $p_4 = 0.77$; $r_5 = 0.10$, $p_5 = 0.72$; $r_6 = 0.08$, $p_6 = 0.65$). BSH07 had only 1 terminal white band so no relationship could be investigated.

3. Cell-based characteristics of white bands in Salix

Normalized CWT averaged from fiber cells within the terminal 100 µm of the tree ring had the highest average correlation with presence of terminal white bands between all trees ($r = 0.68$; Figure 5). Normalized CWT averaged from cells within 50 and 150 µm of the ring boundary had similar but slightly lower average correlations between all trees ($r = 0.63$, $r = 0.67$). Normalized CWT averaged from cells within the last 5% and 10% of each ring also showed correlations within this range ($r = 0.65$, $r = 0.63$). When rings were divided into 8 (12.5% sectors) the correlation strength further decreased ($r = 0.60$)

Correlations between normalized LA and presence of terminal white bands were less than that of CWT for all categories listed above. Normalized LA correlations were highest for cells within the last 5% of the ring ($r = 0.51$). This was followed by normalized LA for cells in the last 10% of the ring ($r = 0.49$), within 150 µm of the ring boundary ($r = 0.47$), the last 12.5% of the ring ($r = 0.46$), within 100 µm of the ring boundary ($r = 0.43$), and within 50 µm of the ring boundary ($r = 0.29$). For every ring-division method and for each cell measurement type, normalizing LA and CWT of each cell to the average LA and CWT for the ring greatly improved the correlation strength.

4. Relationship of CWT to hydrology

As normalized CWT was able to better quantify terminal bands than normalized LA, we focused on this parameter for the remainder of the analysis. We used normalized CWT measurements derived from the last 10% of the ring because it performed nearly as well as using absolute widths and allows better comparisons between rings. In general, there was limited agreement in 10th sector normalized CWT time series between trees (Supplemental Figure 5). Although most relationships were positive, they were largely insignificant. This

precluded our ability to build a site-level chronology for each measurement type. Instead, we compared cell parameter time series for each tree against climatic and hydrologic variables. The most interesting relationships came between normalized CWT and time series of duration (in days) at a particular water level in July. Two trees (BSH03 and BSH05) showed consistent negative correlations around r = 0.4 between normalized CWT and durations for all water levels between 5-10 m (Figure 6). If flooding causes formation of terminal white bands, we expect CWT to decrease as the duration of high water level increases as in these trees. Other trees showed much weaker correlations, or, in the case of BSH01, positive correlations. When comparing normalized CWT to daily water levels for the entire year, we again saw grouping of trees emerge. In particular, trees BSH02/BSH03 and BSH04/BSH05 showed similar relationships with each other. These correlations were quite variable within and between trees. Correlations between CWT and daily mean temperatures and precipitation showed no discernable pattern. There was also no relationship found with 10-day water temperature data.

Discussion

Our results demonstrate that wood fiber CWT is more effective at differentiating between rings with and without terminal white bands than wood fiber LA, especially when normalized by the average CWT for the ring. Terminal white bands clearly have larger LA and lower CWT than cells typically found at the end of the growing season. Although both LA and CWT differed between banded and non-banded rings, the differences were more pronounced with CWT. LA measurements tended to have larger variance within and among trees and this likely reduced its ability to quantify white bands. These differences persisted regardless of the sectoring approach used. This suggests fiber CWT is the preferable measurement for capturing variation in willow rings. In addition, normalization proved valuable for quantifying white bands. Regardless of cell measurement or sectoring approach, normalization improved the correlation strength between cell measurements and the presence of white bands. We therefore recommend that cell measurements are normalized by the average value of the ring in order to better capture unique IADFs.

As for sectoring approaches, using absolute or relative cell positions did not greatly affect our ability to detect terminal white bands. Although average normalized CWT within the terminal 100-150 µm of the ring most strongly correlated with white band presence, it was comparable to using the last 5-10% of each ring. This situation was similar when using normalized LA, which suggests that the two methods, at least for identifying terminal white bands in Salix, are largely comparable. This can be explained, in part, by the fact there were not strong relationships between ring width and white band width. If ring width and white band width were closely related we would expect relative position to outperform absolute position. In general, using relative cell position is appealing because it better accounts for variations in ring width (citations). Since our choice of sectoring approach made little difference in the final results,

we elected to normalize CWT from the last 10% of the ring in our comparisons of flood durations.

Despite multiple indicators that these trees experience flood conditions, we saw no conclusive proof floods were recorded as terminal white bands in *Salix*. Given the height of the island compared to the maximum water levels, as well as the possibly long duration of floods these trees would experience, these trees seemed prime to exhibit a flood response in their rings. SEASCORR results also suggest cold and wet conditions in mid- to late-summer decreased growth. This response appears unusual for an obligate riparian species (e.g., Meko et al., 2015, 2020) but could be due to peak flows in June saturating the soil. Additional moisture while soils are saturated could be producing anoxic conditions, affecting normal root function and reducing growth. Although the strength of these correlations was not extremely strong, they were significant at the highest alpha level (= 0.01). Interestingly, the almost complete absence of terminal white bands after the mid-1980s roughly coincides with a complete lack of water levels of >7 m in July (Figure 3). In the Yenisei River Basin, reservoir operations began in 1981, reducing summer flows in the northern part of the basin (Yang et al., 2004; Stuefer et al., 2011). Given that the chronology responds most strongly to July flows, it seems possible that this hydrological shift is influencing tree growth.

Time series of normalized CWT from the 10th sector did not correlate strongly between trees, largely ruling out the possibility of developing a site-level flood chronology from anatomical measurements. While correlations between cell chronologies were mostly positive, they were extremely weak, suggesting normalized CWT is not recording information at the site level. This idea is further substantiated when correlating normalized CWT with daily water levels and duration time series. Certain pairs of trees showed extremely similar patterns of correlation that were clearly distinct from other trees. These results make the case that CWT in willow is related to the rooting depth of individual trees. We would expect late-season flooding to have a greater impact on trees with deeper root systems, making those trees more likely to form a white band. Although microsite topography can influence both the level and length of time an individual tree is inundated by flood waters, we expect topography to only play a limited role at our site because we observed little elevational difference between trees (~ 1 m). Still, future work should take care to measure elevations of each sampled tree to rule out any influence of topography on the expression of terminal white bands.

Perhaps the most interesting result is the relationship between normalized CWT and number of days water levels exceeded a particular threshold in July (Figure 13). Although most trees showed no correlation to duration, two trees did. The relationship between CWT and flood duration was consistent across water levels, peaking at number of days water levels exceeded 7-8 m (r=-0.4). If longer-duration floods are really the cause of terminal white bands, we would expect this negative correlation, as longer floods would produce rings with thinner fiber cell walls in the last part of the ring. Again, differences in rooting depth

12

may explain why not all trees showed a similar pattern. The complete lack of any patterns in correlations with daily temperature, precipitation, and water temperature leave flooding as the most likely option to explain the presence of terminal white bands in *Salix*.

It is important to note that while July discharge does seem related to tree growth and development of white bands, water levels are not high enough to overtop the island. Given that the island is roughly 12-15 m above the water's surface, and July flows rarely peak above 11 m, it seems unlikely water levels are reaching a point that it is limiting tree growth. In spite of the ring width chronology's negative relationship to July discharge, terminal white bands in some trees appear to be related to water levels maintained at >6 m above the surface of the water, high enough to potentially reach tree roots. As such, July water levels may be important for saturating the soil and root zone with moisture. The terminal white bands, as Yanosky (1984) suggested, may be trees taking advantage of excess moisture at the end of the growing season. Instead of a flood response, July discharge may provide willow on this island an opportunity to add biomass before the end of the growing season.

Alternatively, evidence from physiological studies suggests terminal white bands could be related to a post-flood response in Salix. Work by Mozo et al. (2020) shows flooded Salix grow faster during the post-flood period than their non-flooded counter parts. This is thought to be related to the physiological changes that occur during flooding, including more N in leaves, larger leaf area, more adventitious roots, etc. (Fan et al. 2020). Where flooding tends to reduce ring width and growth, changes to plant physiology during flooding may promote increased growth following disturbance. White bands may not be a flooding response *per se*, but an artifact of physiological changes caused by this disturbance event. It would be useful to compare fiber lumen area and cell wall thickness pre-and post-flood in Salix flooded under experimental conditions to better understand if the changes we see here are a direct or indirect response to large flood events. If this were true, it would have important implications for studies examining flood response in tree rings.

Conclusion

This exploratory analysis not only represents the first time terminal white bands have been quantified using QWA, but is one of only a handful of studies to build time series from measurements of wood fibers in diffuse porous species. We find that normalized fiber cell wall thickness (CWT) is a useful parameter for capturing the IADFs we see in *Salix* rings. Since factors that influence fiber cells may be tree specific, we recommend future work measure the relative elevation of individual trees above the river's surface and any important microtopography. It would also be informative to compare information from wood fibers to that obtained from vessels, which were not investigated in this study. These two sources could be complimentary, allowing us to better understand what role July flows play in ring width formation, and providing a better way to interpret how changes in seasonal flows during the growing season affect willow growth.

ACKNOWLEDGEMENTS

LITERATURE CITED

Agafonov, L.I., Meko, D.M., Panyushkina, I.P., 2016. Reconstruction of Ob River, Russia, discharge from ring widths of floodplain trees. J. Hydrol. 543, 198–207. https://doi.org/10.1016/j.jhydrol.2016.09.031Anadon-Rosell, A., Scharnweber, T., von Arx, G., Peters, R.L., Smiljanić, M., Weddell, S., Wilmking, M., 2022. Growth and wood trait relationships of Alnus glutinosa in peatland forest stands with contrasting water regimes. Front. Plant Sci. 12, 2988. https://doi.org/10.3389/fpls.2021.788106Arbellay, E., Corona, C., Stoffel, M., Fonti, P., Decaulne, A., 2012. Defining an adequate sample of earlywood vessels for retrospective injury detection in diffuse-porous species. PLoS One 7, e38824. https://doi.org/10.1371/journal.pone.0038824Ballesteros-Cánovas, J.A., Stoffel, M., St George, S., Hirschboeck, K., 2015. A review of flood records from tree rings. Prog. Phys. Geogr. 39, 794–816. https://doi.org/10.1177/0309133315608758Ballesteros, J.A., Stoffel, M., Bollschweiler, M., Bodoque, J.M., Díez-Herrero, A., 2010. Flash-flood impacts cause changes in wood anatomy of Alnus glutinosa, Fraxinus angustifolia and Quercus pyrenaica. Tree Physiol. 30, 773–781. https://doi.org/10.1093/TREEPHYS/TPQ031Beck, H.E., Zimmermann, N.E., McVicar, T.R., Vergopolan, N., Berg, A., Wood, E.F., 2018. Present and future köppen-geiger climate classification maps at 1-km resolution. Sci. Data 5, 1–12. https://doi.org/10.1038/sdata.2018.214Bedrick, E.J., 2005. Biserial Correlation. Encycl. Biostat. https://doi.org/10.1002/0470011815.B2A10007Bring, A., Shiklomanov, A., Lammers, R.B., 2017. Pan-Arctic river discharge: Prioritizing monitoring of future climate change hot spots. Earth's Futur. 5, 72–92. https://doi.org/10.1002/eft2.175Brown, M.B., Forsythe, A.B., 1974. Robust Tests for the Equality of Variances. J. Am. Stat. Assoc. 69, 364. https://doi.org/10.2307/2285659Bunn, A.G., 2008. A dendrochronology program library in R (dplR). Dendrochronologia 26, 115–124. https://doi.org/10.1016/J.DENDRO.2008.01.002Buras, A., 2017. A comment on the expressed population signal. Dendrochronologia 44, 130–132. https://doi.org/10.1016/J.DENDRO.2017.03.005Carmack, E.C., Yamamoto-Kawai, M., Haine, T.W.N., Bacon, S., Bluhm, B.A., Lique, C., Melling, H., Polyakov, I. V., Straneo, F., Timmermans, M.L., Williams, W.J., 2016. Freshwater and its role in the Arctic Marine System: Sources, disposition,

storage, export, and physical and biogeochemical consequences in the Arctic and global oceans. J. Geophys. Res. G Biogeosciences 121, 675–717. https://doi.org/10.1002/2015JG003140Coumou, D., Di Capua, G., Vavrus, S., Wang, L., Wang, S., 2018. The influence of Arctic amplification on mid-latitude summer circulation. Nat. Commun. https://doi.org/10.1038/s41467-018-05256-8De Micco, Veronica, Battipaglia, G., Balzano, A., Cherubini, P., Aronne, G., 2016. Are wood fibres as sensitive to environmental conditions as vessels in tree rings with intra-annual density fluctuations (IADFs) in Mediterranean species? Trees - Struct. Funct. 30, 971–983. https://doi.org/10.1007/S00468-015-1338-5/FIGURES/5De Micco, V., Campelo, F., De Luis, M., Bräuning, A., Grabner, M., Battipaglia, G., Cherubini, P., 2016. Intra-annual density fluctuations in tree rings: How, when, where, and why? IAWA J. 37, 232–259. https://doi.org/10.1163/22941932-20160132Edwards, J., Anchukaitis, K.J., Zambri, B., Andreu-Hayles, L., Oelkers, R., D'Arrigo, R., von Arx, G., 2020. Intra-Annual Climate Anomalies in Northwestern North America Following the 1783–1784 CE Laki Eruption. J. Geophys. Res. Atmos. 126, 1–22. https://doi.org/10.1029/2020JD033544Fan, R., Tanekura, K., Morozumi, T., Shingubara, R., Tei, S., Nogovitcyn, A., Starostin, E., Maximov, T.C., Sugimoto, A., 2020. Adaptation of Willows in River Lowlands to Flooding under Arctic Amplification: Evidence from Nitrogen Content and Stable Isotope Dynamics. Wetlands 40, 2413–2424. https://doi.org/10.1007/S13157-020-01353-X/FIGURES/13Feng, D., Gleason, C.J., Lin, P., Yang, X., Pan, M., Ishitsuka, Y., 2021. Recent changes to Arctic river discharge. Nat. Commun. 2021 121 12, 1–9. https://doi.org/10.1038/s41467-021-27228-1Gastwirth, J.L., Gel, Y.R., Miao, W., 2009. The Impact of Levene's Test of Equality of Variances on Statistical Theory and Practice. https://doi.org/10.1214/09-STS301 24, 343–360. https://doi.org/10.1214/09-STS301Gebregeorgis, E.G., Boniecka, J., Piatkowski, M., Robertson, I., Rathgeber, C.B.K., 2021. SabaTracheid 1.0: A Novel Program for Quantitative Analysis of Conifer Wood Anatomy — A Demonstration on African Juniper from the Blue Nile Basin. Front. Plant Sci. 12, 21. https://doi.org/10.3389/fpls.2021.595258He, F., Clark, P.U., 2022. Freshwater forcing of the Atlantic Meridional Overturning Circulation revisited. Nat. Clim. Chang. 2022 125 12, 449–454. https://doi.org/10.1038/s41558-022-01328-2Hogg, E.H., Hart, M., Lieffers, V.J., 2002. White tree rings formed in trembling aspen saplings following experimental defoliation. https://doi.org/10.1139/X02-114Holmes, R., 1983. Computer-Assisted Quality Control in Tree-Ring Dating and Measurement. Tree-ring Bull.IPCC, 2021. Climate Change 2021: The Physical Science Basis. Contribution of Working Group I to the Sixth Assessment Report of the Intergovernmental Panel on Climate Change.Jacobs, P., Viechtbauer, W., 2016. Estimation of the biserial correlation and its sampling variance for use in meta-analysis. https://doi.org/10.1002/jrsm.1218Jones, E.P., Anderson, L.G., Jutterström, S., Mintrop, L., Swift, J.H., 2008. Pacific freshwater, river water and sea ice meltwater across Arctic Ocean basins: Results from the 2005 Beringia Expedition. J. Geophys. Res. 113, 1–10. https://doi.org/10.1029/2007jc004124Kames, S., Tardif, J.C., Bergeron, Y., 2016. Continuous earlywood vessels chronolo-

gies in floodplain ring-porous species can improve dendrohydrological reconstructions of spring high flows and flood levels. J. Hydrol. 534, 377–389. https://doi.org/10.1016/J.JHYDROL.2016.01.002López, J., Del Valle, J.I., Giraldo, J.A., 2014. Flood-promoted vessel formation in Prioria copaifera trees in the Darien Gap, Colombia. Tree Physiol. 34, 1079–1089. https://doi.org/10.1093/TREEPHYS/TPU077MacDonald, G.M., Kremenetski, K. V., Smith, L.C., Hidalgo, H.G., 2007. Recent Eurasian river discharge to the Arctic Ocean in the context of longer-term dendrohydrological records. J. Geophys. Res. Biogeosciences 112. https://doi.org/10.1029/2006JG000333Meko, D.M., Friedman, J.M., Touchan, R., Edmondson, J.R., Griffin, E.R., Scott, J.A., 2015. Alternative standardization approaches to improving streamflow reconstructions with ring-width indices of riparian trees. Holocene 25, 1093–1101. https://doi.org/10.1177/0959683615580181Meko, D.M., Panyushkina, I.P., Agafonov, L.I., Edwards, J.A., 2020. Impact of high flows of an Arctic river on ring widths of floodplain trees. Holocene 30, 789–798. https://doi.org/10.1177/0959683620902217Meko, D.M., Touchan, R., Anchukaitis, K.J., 2011. Seascorr: A MATLAB program for identifying the seasonal climate signal in an annual tree-ring time series. Comput. Geosci. 37, 1234–1241. https://doi.org/10.1016/J.CAGEO.2011.01.013Meko, D.M., Woodhouse, C.A., Morino, K., 2012. Dendrochronology and links to streamflow. J. Hydrol. 412–413, 200–209. https://doi.org/10.1016/j.jhydrol.2010.11.041Meko, M.D., Therrell, M.D., 2020. A record of flooding on the White River, Arkansas derived from tree-ring anatomical variability and vessel width. Phys. Geogr. 41, 83–98. https://doi.org/10.1080/02723646.2019.1677411Nolin, A.F., Tardif, J.C., Conciatori, F., Kames, S., Meko, D.M., Bergeron, Y., 2021. Multi-century tree-ring anatomical evidence reveals increasing frequency and magnitude of spring discharge and floods in eastern boreal Canada. Glob. Planet. Change 199, 103444. https://doi.org/10.1016/J.GLOPLACHA.2021.103444Panyushkina, I.P., Meko, D., Shiklomanov, A., Thaxton, R., Myglan, V., Barinov, V. V, Taynik, A. V, 2021. Unprecedented acceleration of winter discharge of Upper Yenisei River inferred from tree rings. Environ. Res. Lett. https://doi.org/10.1088/1748-9326/ac3e20Peters, R.L., Balanzategui, D., Hurley, A.G., Von Arx, G., Prendin, A.L., Cuny, H.E., Björklund, J., Frank, D.C., Fonti, P., 2018. RAPTOR: Row and position tracheid organizer in R. Dendrochronologia 47, 10–16. https://doi.org/10.1016/j.dendro.2017.10.003Porter, C., Morin, P., Howat, I., Noh, M.-J., Bates, B., Peterman, K., Keesey, S., Schlenk, M., Gardiner, J., Tomko, K., Willis, M., Kelleher, C., Cloutier, M., Husby, E., Foga, S., Nakamura, H., Platson, M., Wethington, M.J., Williamson, C., Bauer, G., Enos, J., Arnold, G., Kramer, W., Becker, P., Doshi, A., D'Souza, C., Cummens, P., Laurier, F., Bojesen, M., 2018. ArcticDEM [WWW Document]. Harvard Dataverse, V1. https://doi.org/https://doi.org/10.7910/DVN/OHHUKHPrendin, A.L., Carrer, M., Karami, Mojtaba, Hollesen, J., Nanna, , Pedersen, B., Pividori, M., Urs, , Treier, A., Westergaard-Nielsen, A., Elberling, B., Normand, S., 2020. Immediate and carry-over effects of insect outbreaks on vegetation growth in West Greenland assessed from cells to satellite. J. Biogeogr. 47.

https://doi.org/10.1111/jbi.13644Rizopoulos, D., 2007. ltm: An R Package for Latent Variable Modeling and Item Response Analysis. J. Stat. Softw. 17, 1–25. https://doi.org/10.18637/JSS.V017.I05Royston, P., 1995. Remark AS R94: A Remark on Algorithm AS 181: The W-test for Normality. Appl. Stat. 44, 547. https://doi.org/10.2307/2986146Screen, J.A., Simmonds, I., 2010. The central role of diminishing sea ice in recent Arctic temperature amplification. Nature 464, 1334–1337. https://doi.org/10.1038/nature09051Serreze, M.C., Francis, J.A., 2006. The Arctic on the fast track of change. Weather 61, 65–69. https://doi.org/10.1256/wea.197.05Shapiro, S.S., Wilk, M.B., 1965. An Analysis of Variance Test for Normality (Complete Samples). Biometrika 52, 591. https://doi.org/10.2307/2333709Shiklomanov, A.I., Lammers, R.B., 2009. Record Russian river discharge in 2007 and the limits of analysis. Environ. Res. Lett. 4, 1–9. https://doi.org/10.1088/1748-9326/4/4/045015Shiklomanov, A.I., Lammers, R.B., Lettenmaier, D.P., Polischuk, Y.M., Savichev, O.G., Smith, L.C., Chernokulsky, A. V., 2013. Hydrological Changes: Historical Analysis, Contemporary Status, and Future Projections, in: Regional Environmental Changes in Siberia and Their Global Consequences. Springer, Dordrecht, pp. 111–154. https://doi.org/10.1007/978-94-007-4569-8_4Smith, L.C., Stephenson, S.R., 2013. New Trans-Arctic shipping routes navigable by midcentury. PNAS 110, E1191–E1195. https://doi.org/10.1073/pnas.1214212110Stokes, M., Smiley, T., 1968. An Introduction to Tree Ring Dating. University of Chicago Press, Chicago.Stuefer, S., Yang, D., Shiklomanov, A., 2011. Effect of streamflow regulation on mean annual discharge variability of the Yenisei River 346.Tardif, J.C., Dickson, H., Conciatori, F., Nolin, A.F., Bergeron, Y., 2021. Are periodic (intra-annual) tangential bands of vessels in diffuse-porous tree species the equivalent of flood rings in ring-porous species? Reproducibility and cause. Dendrochronologia 70, 125889. https://doi.org/10.1016/J.DENDRO.2021.125889Tyree, M.T., Ewers, F.W., 1991. The hydraulic architecture of trees and other woody plants. New Phytol. 119, 345–360. https://doi.org/10.1111/j.1469-8137.1991.tb00035.xvon Arx, G., Carrer, M., 2014. ROXAS-A new tool to build centuries-long tracheid-lumen chronologies in conifers. Dendrochronologia 32, 290–293. https://doi.org/10.1016/j.dendro.2013.12.001von Arx, G., Kueffer, C., Fonti, P., 2013. Quantifying plasticity in vessel grouping - Added value from the image analysis tool ROXAS. IAWA J. 34, 433–445. https://doi.org/10.1163/22941932-00000035Wegner, L., Eilmann, B., Sass-Klaassen, U., Von Arx, G., 2013. ROXAS – an efficient and accurate tool to detect vessels in diffuse-porous species. IAWA J. 34, 425–432. https://doi.org/10.1163/22941932-00000034Weijer, W., Cheng, W., Garuba, O.A., Hu, A., Nadiga, B.T., 2020. CMIP6 Models Predict Significant 21st Century Decline of the Atlantic Meridional Overturning Circulation. Geophys. Res. Lett. 47. https://doi.org/10.1029/2019GL086075Wickham, H., 2009. ggplot2. ggplot2. https://doi.org/10.1007/978-0-387-98141-3Yamaguchi, D.K., 2011. A simple method for cross-dating increment cores from living trees. https://doi.org/10.1139/x91-053 21, 414–416. https://doi.org/10.1139/X91-053Yang, D., Ye, B., L. Kane, D., 2004.

Streamflow changes over Siberian Yenisei River Basin. J. Hydrol. 296, 59–80. https://doi.org/10.1016/J.JHYDROL.2004.03.017Yanosky, T.M., 1984. Documentation of high summer flows on the Potomac River from the wood anatomy of ash trees. J. Am. Water Resour. Assoc. 20, 241–250. https://doi.org/10.1111/j.1752-1688.1984.tb04678.xZanowski, H., Jahn, A., Holland, M.M., 2021. Arctic Ocean Freshwater in CMIP6 Ensembles: Declining Sea Ice, Increasing Ocean Storage, and Export. J. Geophys. Res. Ocean. 126, e2020JC016930. https://doi.org/10.1029/2020JC016930
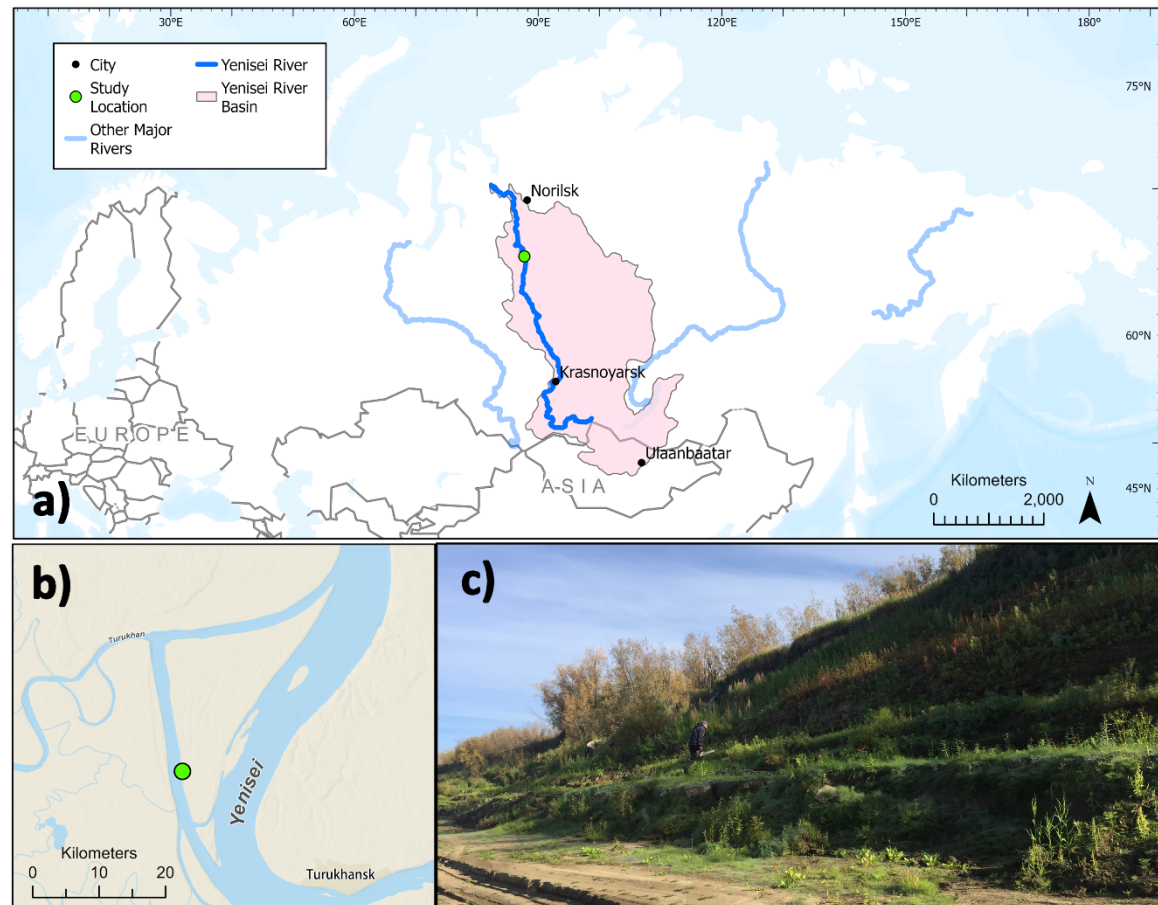
FIGURES

Figure 1. Illustration of the study site. Panel a) shows the geographic location of the Yenisei River basin (pink polygon) and Yenisei River (dark blue line) in relation to other major Arctic rivers (light blue). The study location is shown as a green dot. b) Location of the study site in relation to island at the confluence of the Turukhan and Yenisei Rivers. The study site is roughly 10 km downstream from the town of Turukhansk. c) Vertical profile of island. The riparian forest

sampled rests at the top of a terraced island. The height of the island is roughly 12-15 m above the water's surface, estimated using the online tool ArcticDEM (Porter et al., 2018).
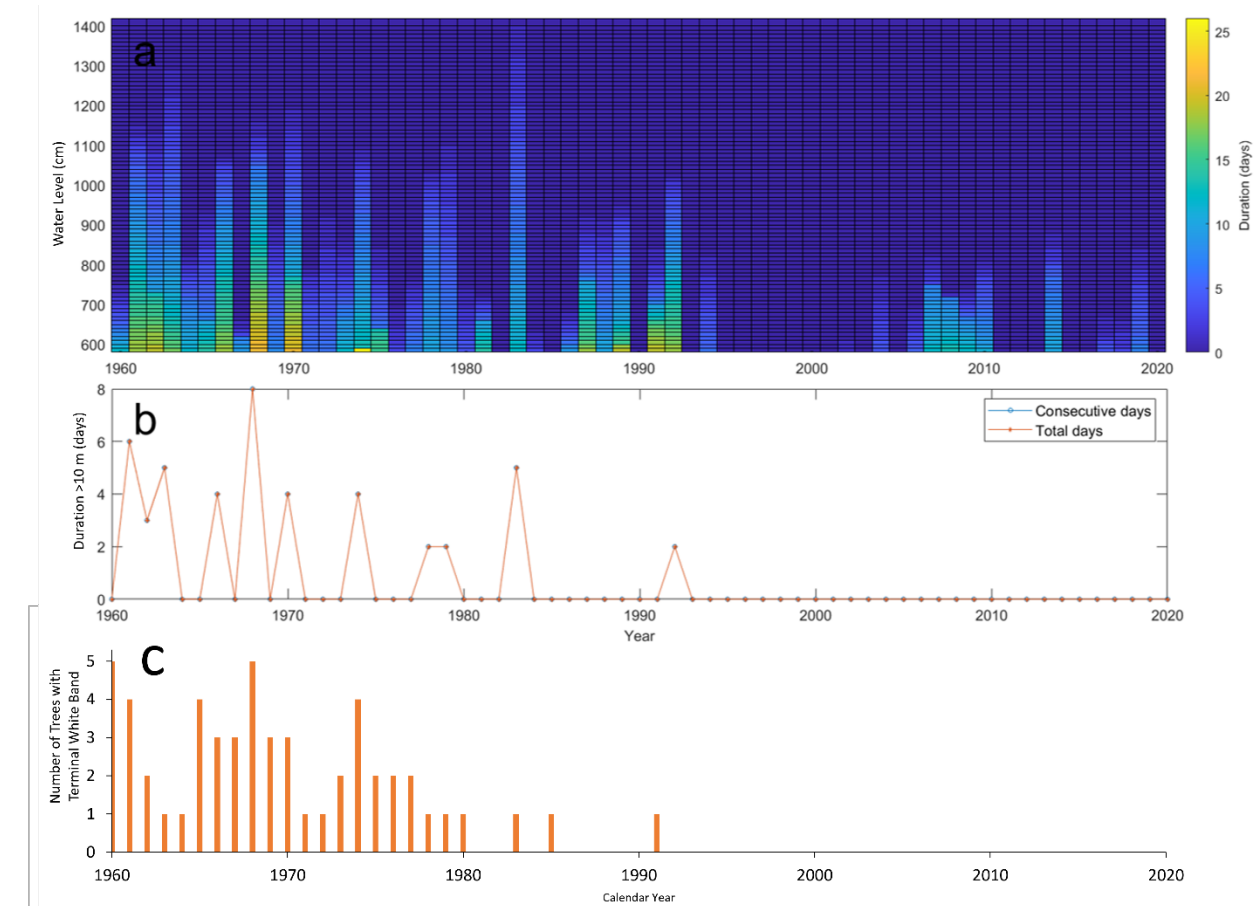

Figure 2. July daily water levels and durations at Selivanikha (gauge code 9801), 1960-2020. The zero water level for this gage is 1.26 meters above sea level. Gauge location is just downstream of the study site and 6 km east. a) Number of days water levels reached a particular value. July water levels do not exceed 14 meters and water levels above 7 meters do not typically last longer than 15 days. b) Time series of total days and consecutive days water level fell above 10 meters. No data available for years 1993, 1995-98, and 2000-01. c) Frequency histogram with the number of trees that contained a terminal white band (orange bars) IADF in a particular year.

19
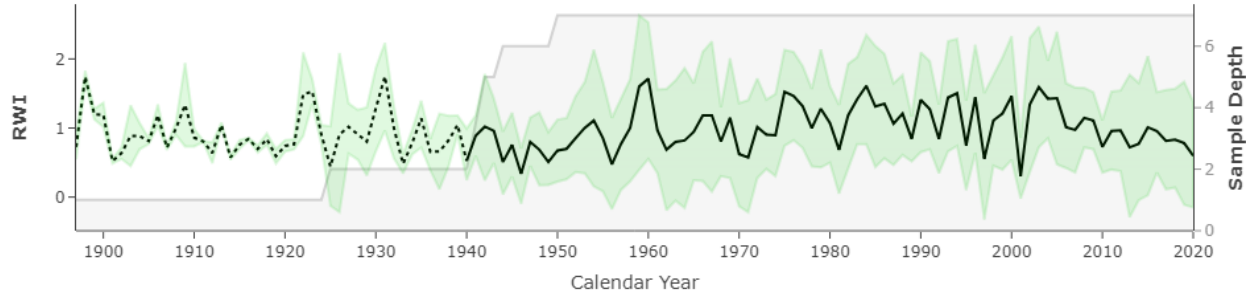
Figure 3. Detrended tree ring width chronology, 1897-2020. Black line is average ring width increment, where dotted portion indicates where sub-sample signal strength falls below 0.9. Tree ring width detrended using dplR (Bunn, 2008). Green ribbon is the 95% confidence interval (i.e. all values within 2 standard deviations of the mean value of the chronology in that year). Gray polygon indicates sample depth in a particular year.
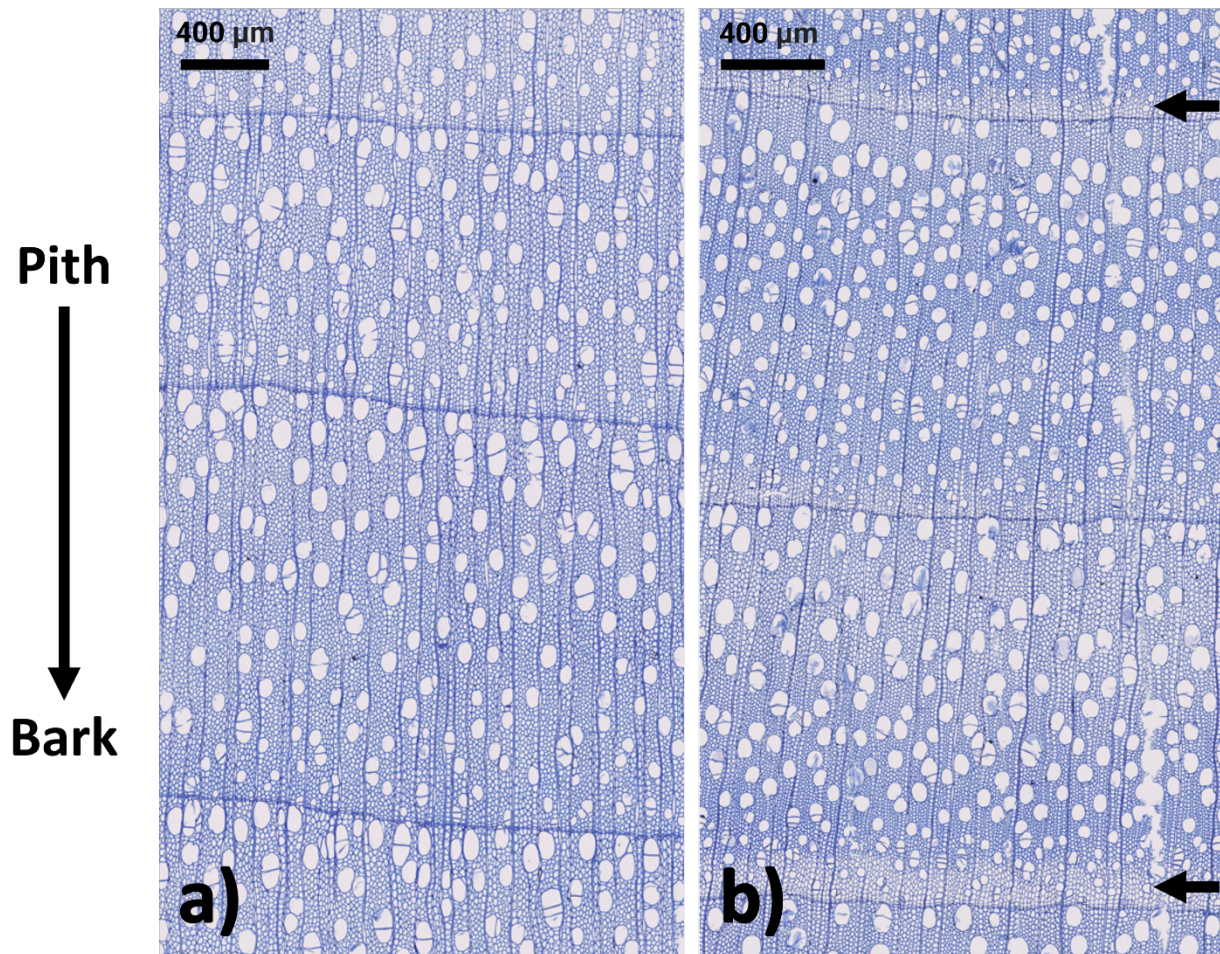
Figure 4. Comparison of rings with and without terminal white bands. White bands are a type of intra-annual density fluctuation (IADF), or regions where abrupt changes in density occur (V. De Micco et al., 2016). Rings are progressively older from the top to bottom of the image. a) Rings 2017-2020 from tree BSH01. These years do not show a terminal white band, as there is little variation in wood fibers over the width of the ring. b) Rings 1955-1958 from tree BSH03. Years 1955 and 1957 show distinct terminal white bands (black arrows).

Normalized CWT
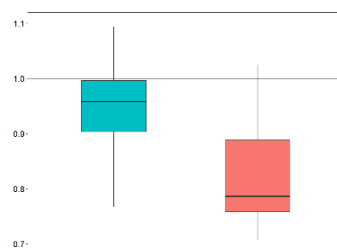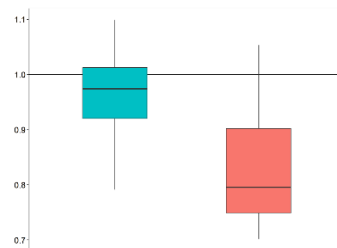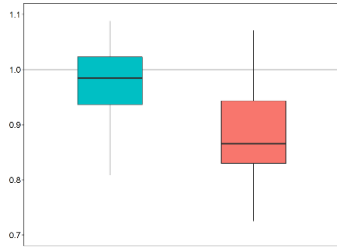
Normalized LA
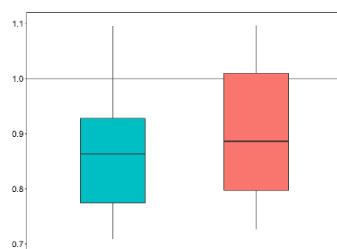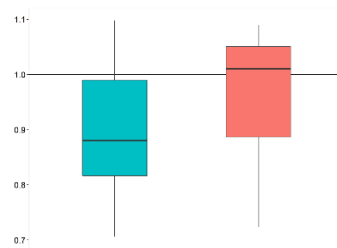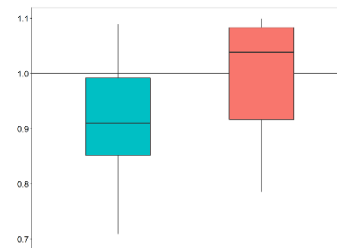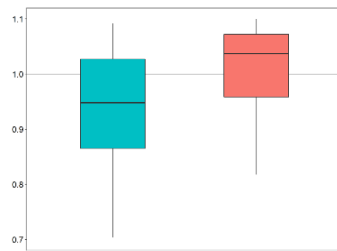
>87.5% of ring

>90% of ring

>95% of ring

Last 150 μm

Last 100 μm

Last 50 μm

No Terminal
White Band

Terminal
White Band

No Terminal
White Band

Terminal
White Band

22

Figure 5. Comparison of normalized CWT and LA measurements for years without (n = 185; blue boxplots) and with (n = 92; red boxplots) terminal white bands, 1947-1986. Each row indicates the sectoring method (absolute vs relative cell positions) to capture terminal white band. Horizontal line at y = 1 is the average expected value. Cell parameters for each ring were normalized by dividing each cell measurement by the average cell measurement value for the entire ring. Years where we visually identified terminal white bands tend to have lower fiber CWT values and higher fiber LA values for most trees. In general, there is more variation in fiber LA than CWT. The difference between rings with and without terminal white bands is highly significant (p « 0.001, 2-sample t-test) for all combinations of cell parameters and sectoring method. For comparison of rings with and without terminal white bands by tree, see Supplemental Figure 5.
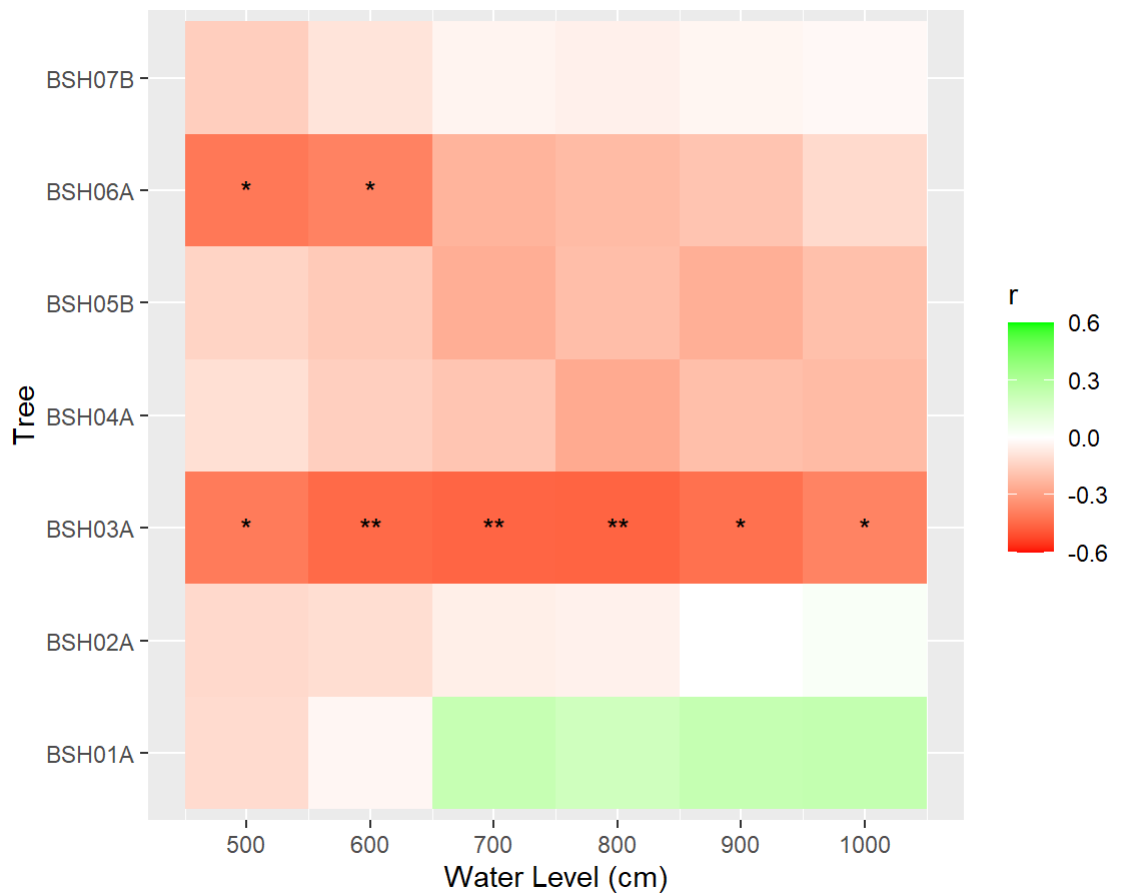

Figure 6. Correlation between normalized cell wall thickness (CWT) in the 10th sector and water level duration for each tree (1960-1980). The x-axis indicates water level for the month of July and the y-axis indicates the tree. The color in

23

cell indicates the correlation between the normalized CWT time series for each tree and the consecutive number of days at or above that particular water level. Green cells indicate positive correlations, red cells indicate negative correlations, and the intensity of the color indicates the correlation strength. The number of asterisks (*) refers to the significance level (*: $0.05 <= p <= 0.1$, **: $0.01 <= p <= 0.05$).

TABLES

| Tree	Pith Year	Years with Early IADFs (1950-2020)	Years with Late IADFs (1950-2020)	Years with ROXAS Data
BSH01	1941	5	11	1965-1981
BSH02	1925	0	17	1947-1983
BSH03	1942	3	21	1949-1986
BSH04	1945	17	23	1960-1980
BSH05	1942	7	17	1965-1981
BSH06	1897	4	8	1956-1983
BSH07	1951	0	1	1964-1983

Table 1. List of sampled *Salix alba* trees. For each tree the pith year (earliest ring), number of years with visually-identified early and late IADFs, and the span of time with ROXAS data is shown.

SUPPLEMENTARY FIGURES
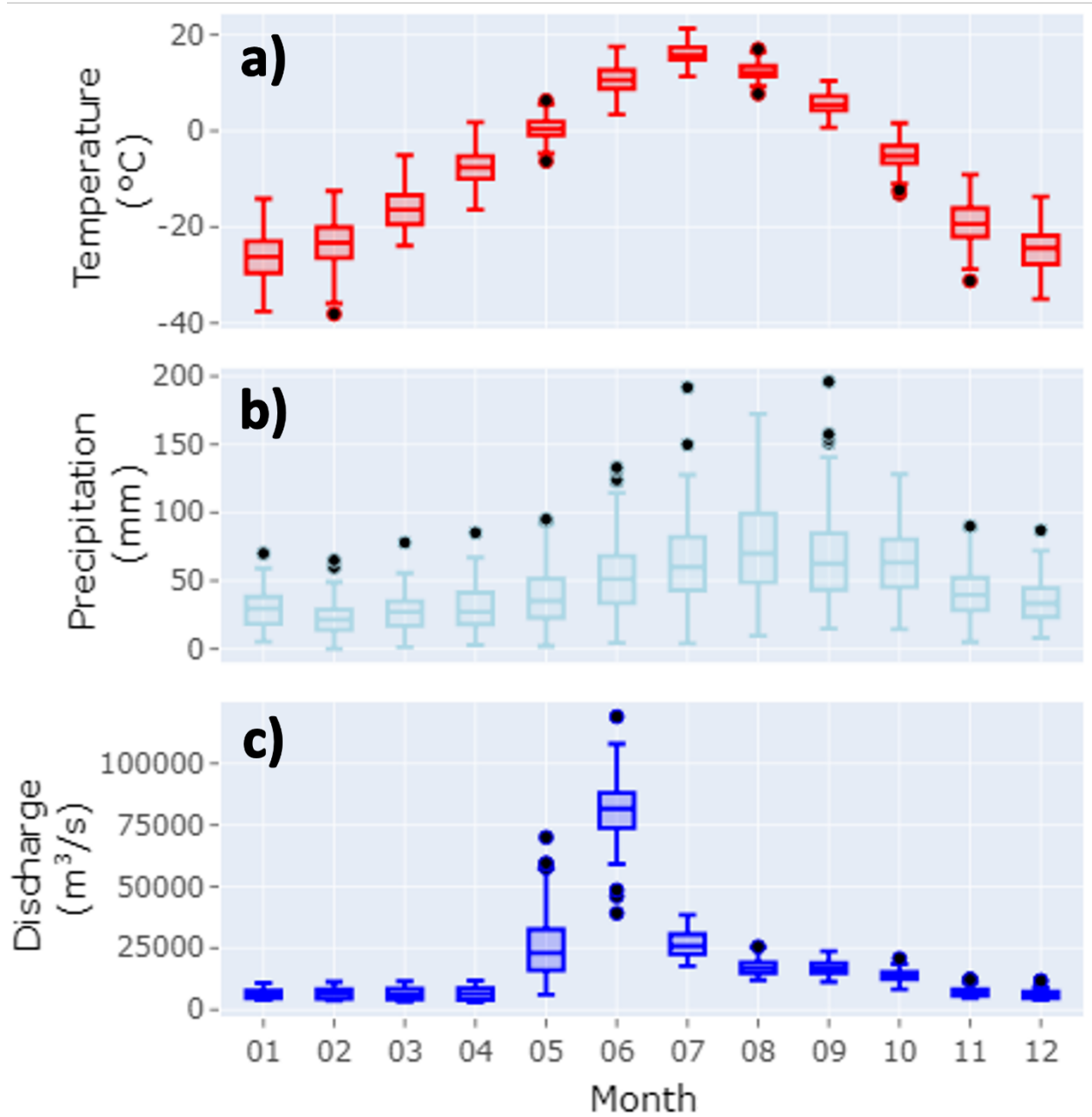
Supplemental Figure 1. Monthly climograph and hydrograph. a) Average monthly temperature in Celsius from Turukhansk (WMO Code 23472), 1926-2018 b) Average total monthly precipitation in millimeters from Turukhansk (WMO Code 23472), 1912-2017 c) Average monthly discharge in cubic meters

pers second from Yenisey at Igarka gauge (9803), 1936-1999.
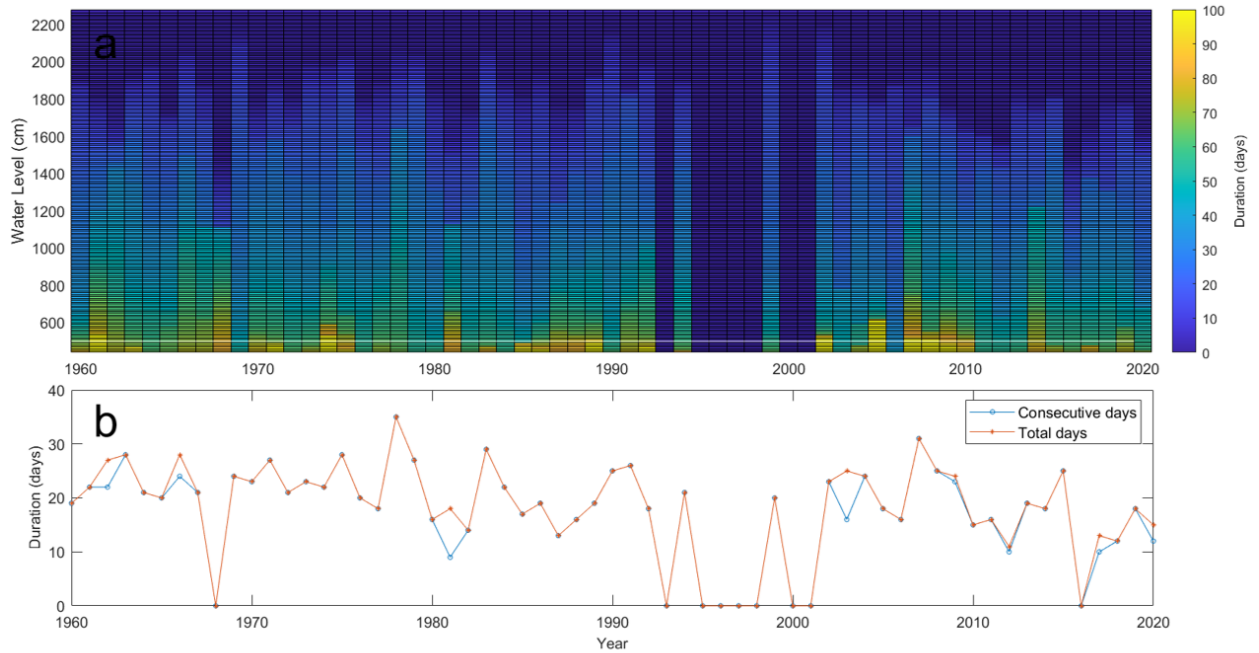
Supplemental Figure 2: Annual water levels and durations at Selivanikha (9801), 1960-2020. a) Number of days water levels reached a particular value. Annual water levels do not exceed 22 meters at this study site and water levels above 14 meters do not typically last longer than 30 days. In contrast b) Time series of total days and consecutive days water level fell above 15 meters. No data available for years 1993, 1995-98, and 2000-01.
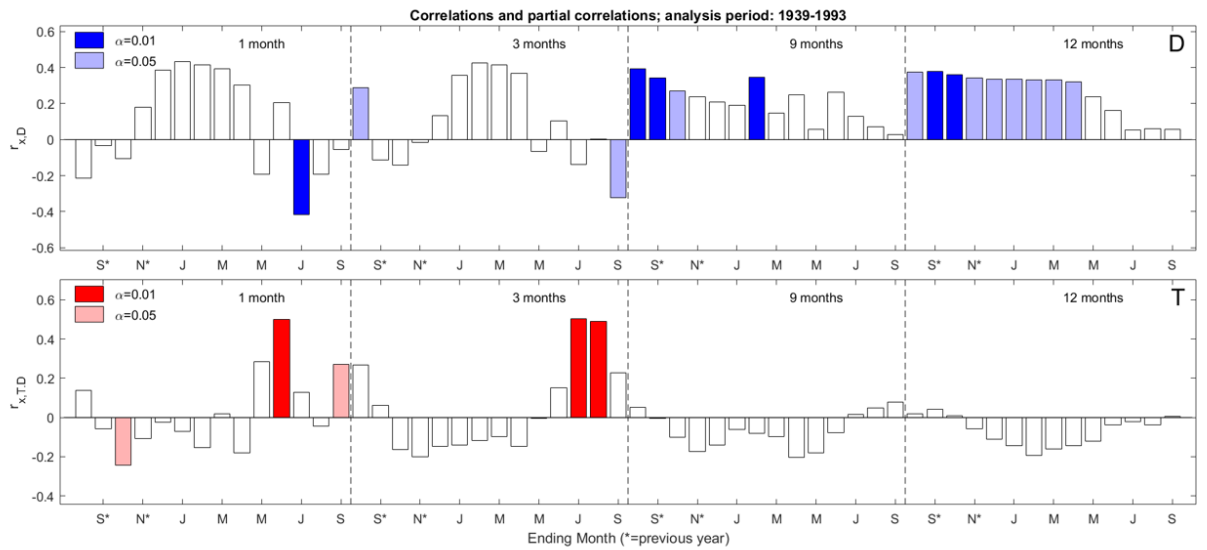
Supplemental Figure 3: SEASCORR results, 1939-1993. Partial correlations between detrended tree ring width chronology and Yenisey at Igarka monthly discharge, station code 9803, (blue, primary variable), and Turukhansk mean monthly temperature (red, secondary variable) over common interval.
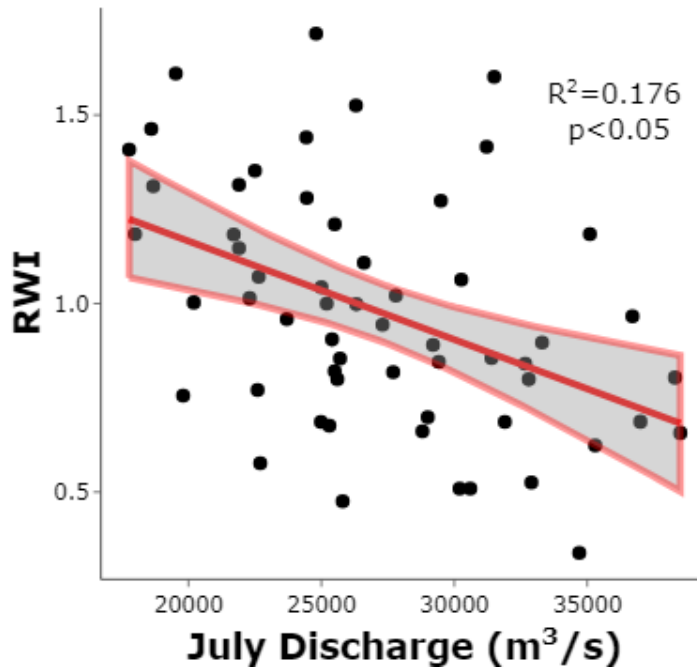
Supplemental Figure 4. Scatterplot of July discharge, in cubic meters per second, and tree growth (1938-1993). The strongest single-month correlations between tree growth and discharge is with the month of July. The negative relationship is significant (r = 0.18, p < 0.05) and suggests tree radial growth decreases as discharge increases. Red line is linear fit of the data. Grey polygon with red outline is confidence band of the linear fit.

Normalized CWT

Normalized LA

50 micron

100 micron

150 micron

12.5% of ring

10% of ring

5% of ring
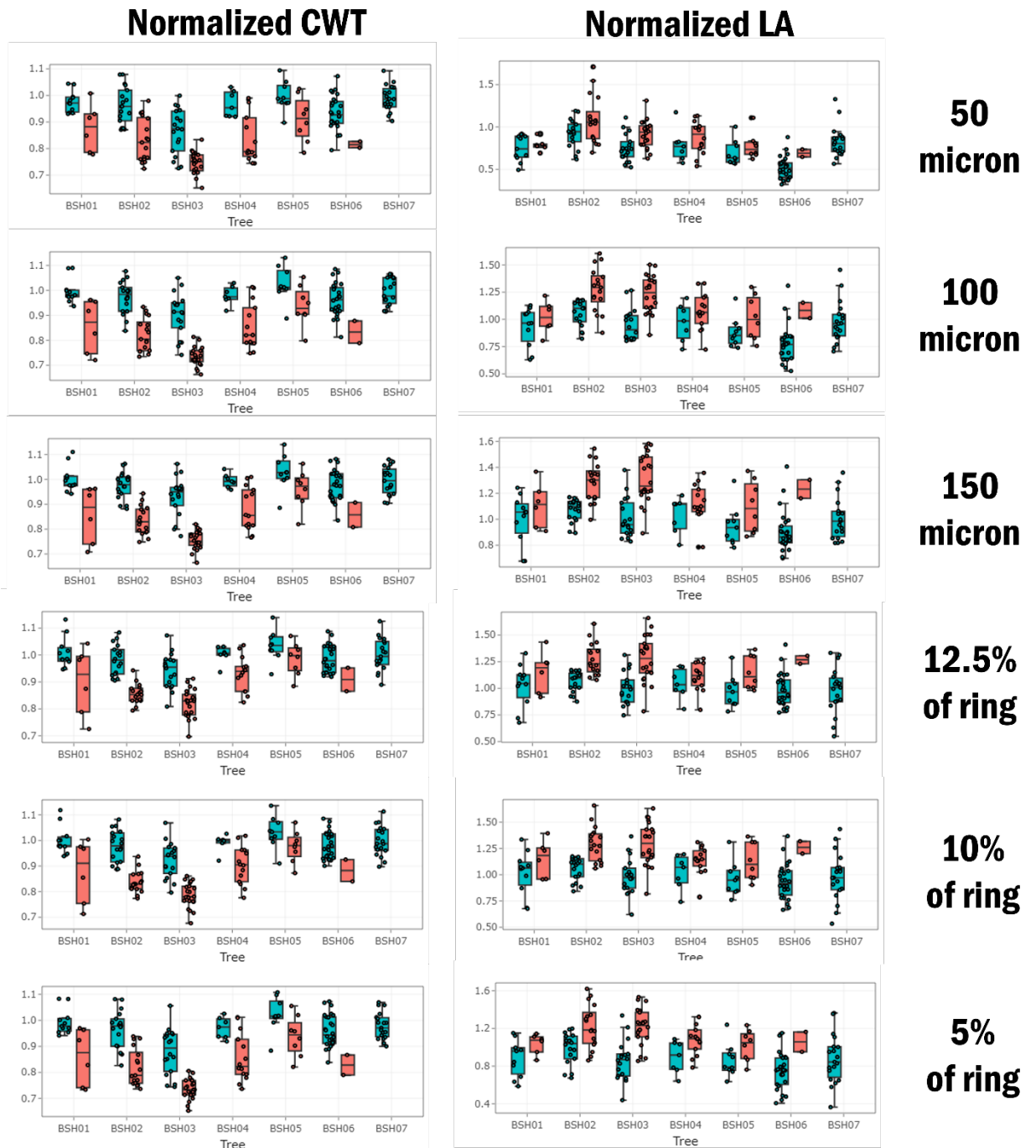
Supplemental Figure 5: Comparison of normalized CWT and LA measurements

for years without (blue boxplots) and with (red boxplots) terminal white bands by tree, 1947-1986. Each row indicates the sectoring method (absolute vs relative cell positions) to capture terminal white band. Horizontal line at $y = 1$ is the average expected value. Cell parameters for each ring were normalized by dividing each cell measurement by the average cell measurement value for the entire ring. Years where we visually identified terminal white bands tend to have lower fiber CWT values and higher fiber LA values for most trees.
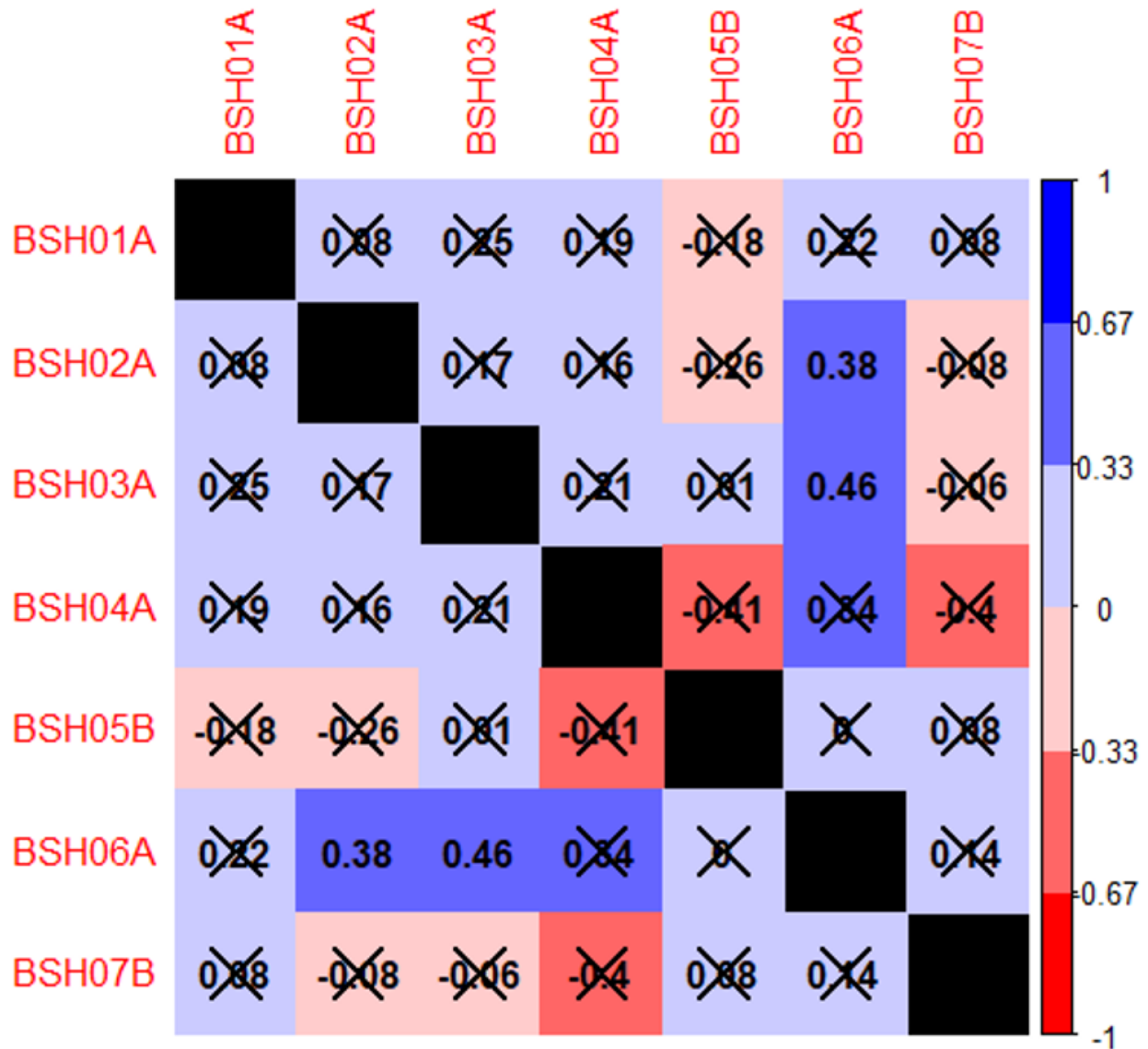
Supplemental Figure 5. Correlation matrix of normalized CWT series from 10th sector of each tree. Time series of normalized CWT were compared using Pearson correlations for each possible pair of trees. Blue boxes indicate positive correlations, red boxes indicated negative correlations and the intensity of the color denotes the strength of the correlation. Boxes with non-significant correlations contain a black 'X'.